Electronic Supplementary Information

Dithieno[3,2-*b*:2',3'-*d*]pyridin-5(4*H*)-one-based polymers with bandgap up to 2.02 eV for high performance field-Effect transistors and polymer solar cells with open-circuit voltage up to 0.98 V and efficiency up to 6.84%

Minghui Hao,[a] Guoping Luo,[b] Keli Shi,[c] Guohua Xie,[a] Kailong Wu,[a] Hongbin Wu,[,b] Gui Yu,*[,c] Yong Cao, and Chuluo Yang*[,a]*

[a] Hubei Collaborative Innovation Center for Advanced Organic Chemical Materials, Hubei Key Lab on Organic and Polymeric Optoelectronic Materials, Department of Chemistry, Wuhan University, Wuhan 430072, China.

[b] Institute of Polymer Optoelectronic Materials and Devices, State Key Laboratory of Luminescent Materials and Devices, South China University of Technology, Guangzhou 510640, China.

[c] Beijing National laboratory for Molecular Sciences, Key Laboratory of Organic Solids, Institute of Chemistry, Chinese Academy of Sciences, Beijing 100080, China.

Table of Contents

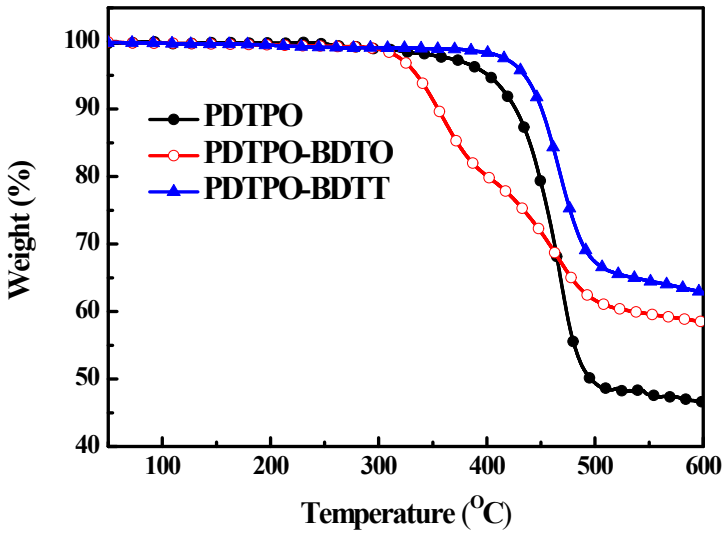

Fig. S1 TGA plots of the polymers with a heating rate of 10 K/min under the nitrogen atmosphere.

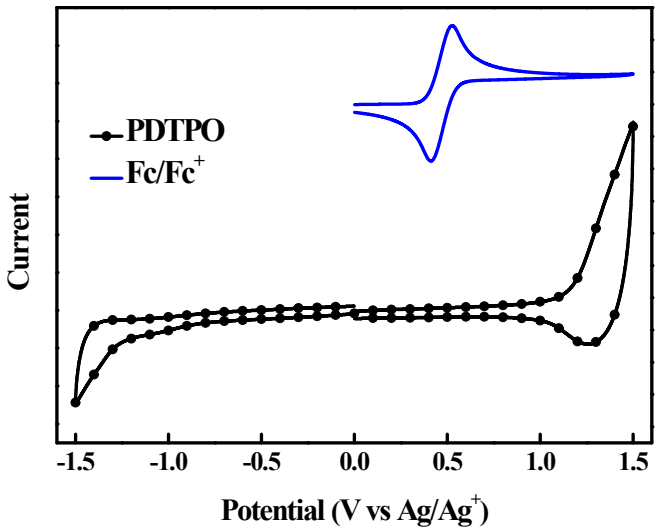

Fig. S2 Cyclic voltammogram of PDTPO thin film coated onto a platinum plate in an acetonitrile solution of 0.1 M *n*-Bu_4NPF_6 at a scan rate of 100 mV s^{-1}.

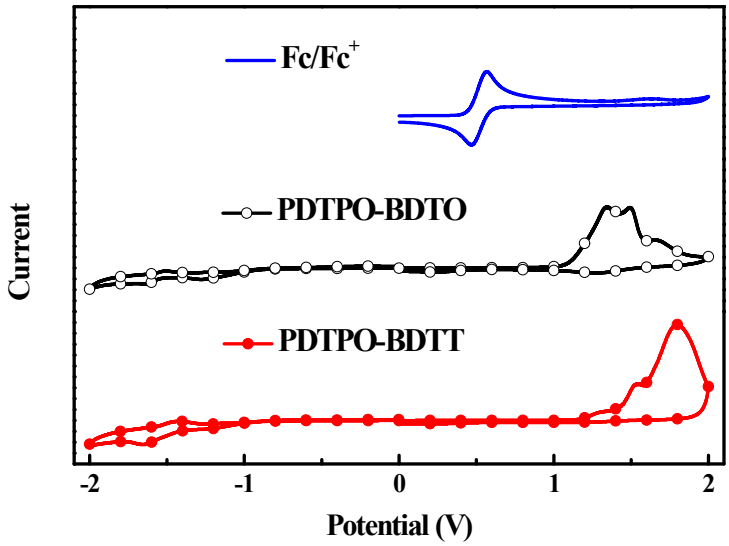

Fig. S3 Cyclic voltammogram of PDTPO-BDTO and PDTPO-BDTT thin films coated onto a platinum plate in an acetonitrile solution of 0.1 M *n*-Bu_4NPF_6 at a scan rate of 100 mV s^{-1}.

Table S1. OFET hole mobility of PDTPO at different annealing temperatures.

Condition	As-cast	80 °C	160 °C	240 °C
mobility ($cm^2\ V^{-1}\ s^{-1}$)	0.011	0.033	0.04	0.19

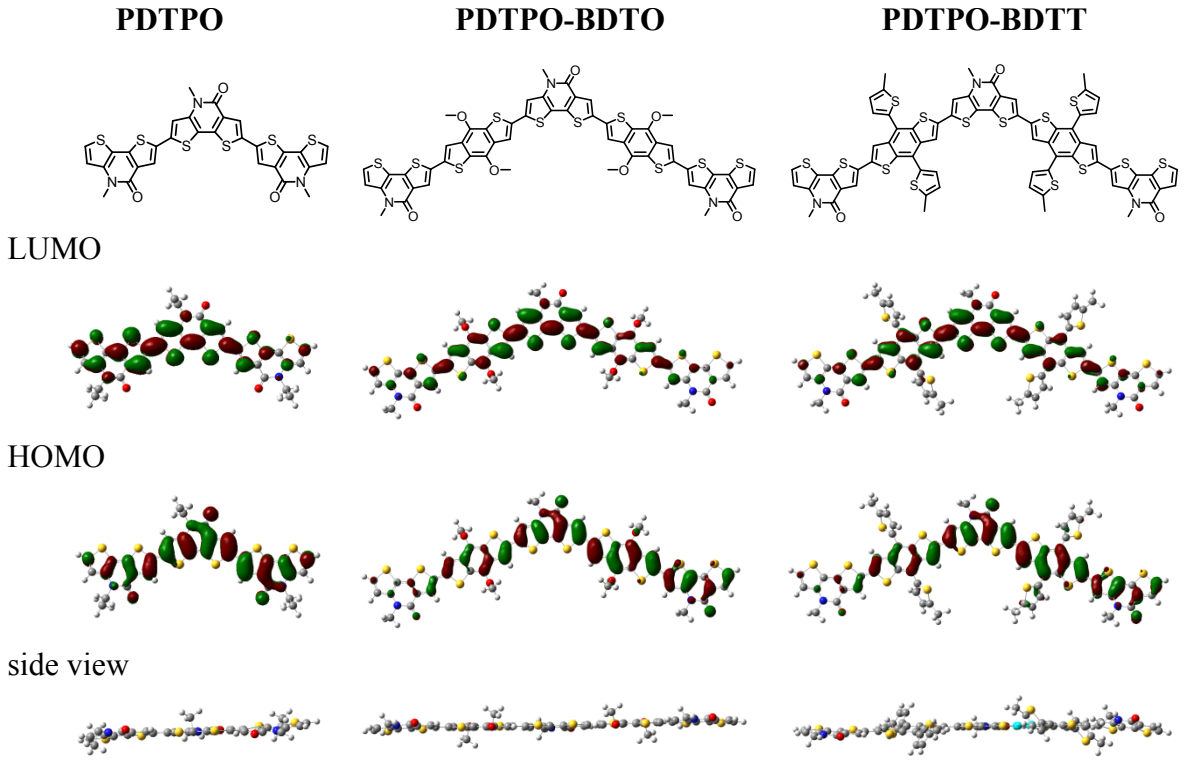

Fig. S4 DFT calculations of the trimer of PDTPO, and five units of PDTPO-BDTO and PDTPO-BDTT.

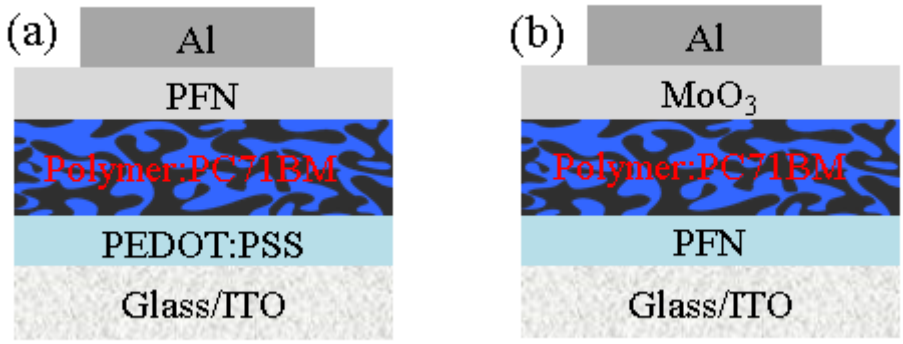

Fig. S5 The structure of the conventional (a) and inverted (b) devices investigated in this work.

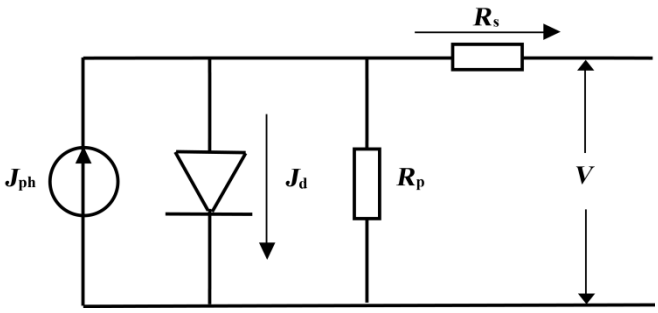

Fig. S6 Equivalent circuit model of the polymer solar cell under illumination.

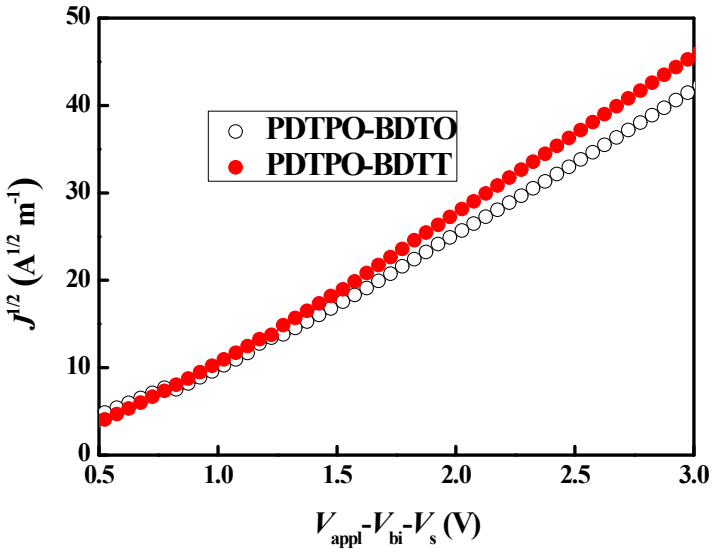

Fig. S7 Current density-voltage characteristics of PDTPO-BDTO and PDTPO-BDTT blends with $PC_{71}BM$ in SCLC devices.

Table S2. The extracted electrical parameters of the conventional devices based on the *J-V* characteristics of Fig. 5a and 5b.

polymer		PDTPO-BDTO	PDTPO-BDTO
as cast [a]	R_s [b] (Ω cm^2)	2.15	9.40
	R_p [b] (Ω cm^2)	7.44×10^2	9.19×10^4
	n	4.65	5.92
THF 0 s + PFN [a]	R_s [b] (Ω cm^2)	2.64	0.10
	R_p [b] (Ω cm^2)	1.19×10^3	1.48×10^3
	n	3.02	3.25
THF 30 s + PFN [a]	R_s [b] (Ω cm^2)	2.86	2.72
	R_p [b] (Ω cm^2)	1.49×10^3	1.64×10^3
	n	2.22	2.27
THF 60 s + PFN [a]	R_s [b] (Ω cm^2)	1.27	1.86
	R_p [b] (Ω cm^2)	1.16×10^3	4.10×10^2
	n	2.88	2.33

[a] Fitting with the equation (1) based on the equivalent circuit model illustrated in Fig. S6. [b] R_s (series resistance) and R_p (parallel resistance) are extracted by the fitting and these two values are different from those calculated from the slopes of the *J-V* curves at $J = 0$ and $V = 0$ under illumination.

$$J = J_{ph} - J_0[\exp(\frac{V + JR_s}{nkT/q}) - 1] - \frac{V + JR_s}{R_p} \quad (1)$$

where J_{ph} is the photocurrent, J_0 the diode saturation current, n the diode quality factor, R_s the series resistance, and R_p the parallel (shunt) resistance.

Table S3. The extracted electrical parameters of the inverted devices.

polymer	R_s (Ω cm^2)	R_p (Ω cm^2)	n
PDTPO-BDTO	1.99	9.83×10^4	4.92
PDTPO-BDTT	3.43	8.98×10^4	3.42

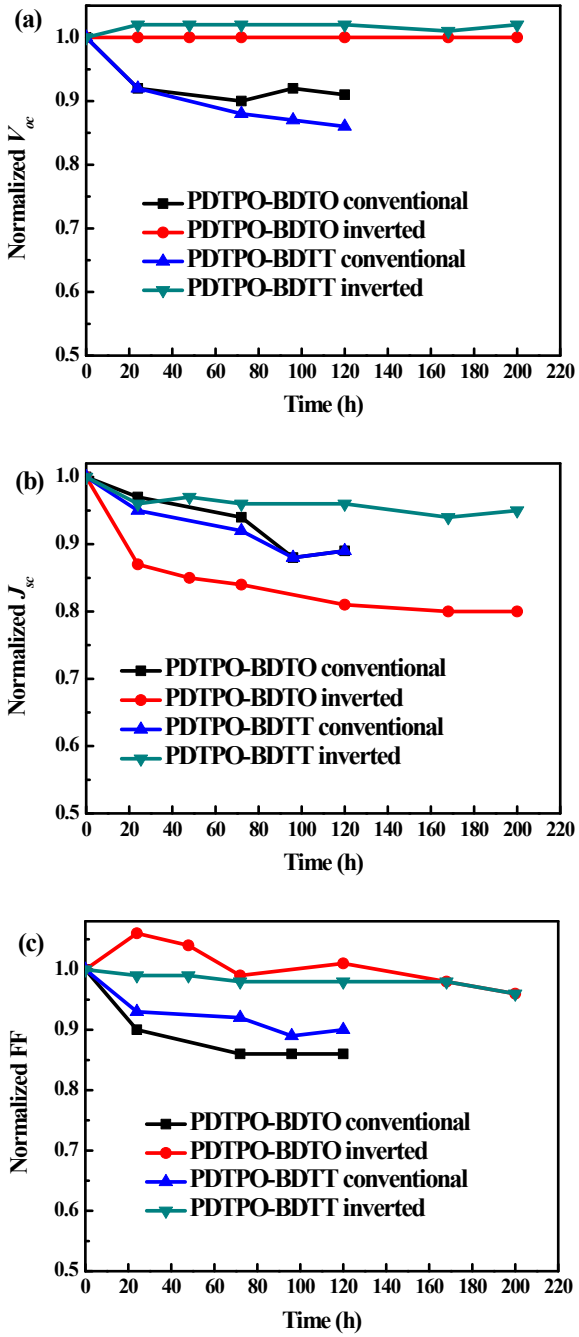

Fig. S8 Stability curves of the PDTPO-BDTO and PDTPO-BDTT devices versus storage time in air. (a) normalized V_{oc}, (b) normalized J_{sc}, (c) normalized FF.

Table S4. Normalized conventional device performance after 120 h of ageing in air.

	V_{oc} (V)	J_{sc} (mA cm^{-2})	FF	PCE
PDTPO-BDTO	0.91	0.89	0.86	0.70
PDTPO-BDTT	0.86	0.89	0.90	0.68

Table S5. Normalized inverted device performance after 200 h of ageing in air.

	V_{oc} (V)	J_{sc} (mA cm^{-2})	FF	PCE
PDTPO-BDTO	1.00	0.80	0.96	0.77
PDTPO-BDTT	1.02	0.95	0.96	0.93

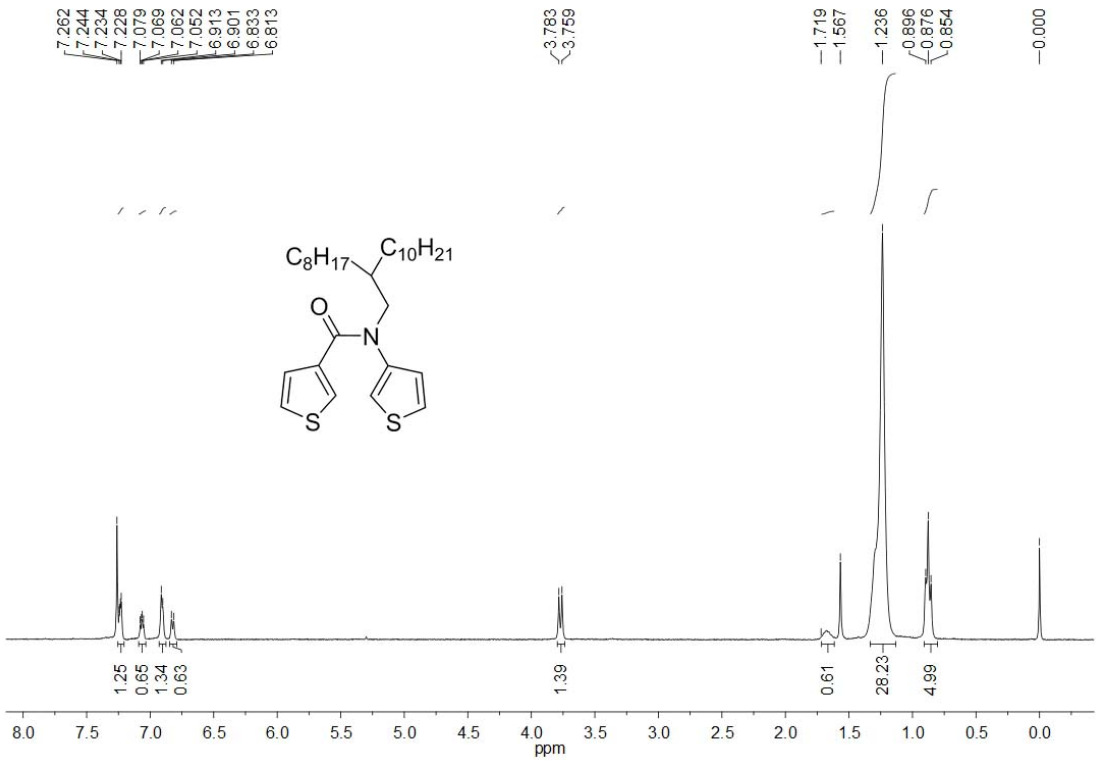

Fig. S9 [1]H NMR spectrum of **2** conducted in *d*-chloroform at 298K.

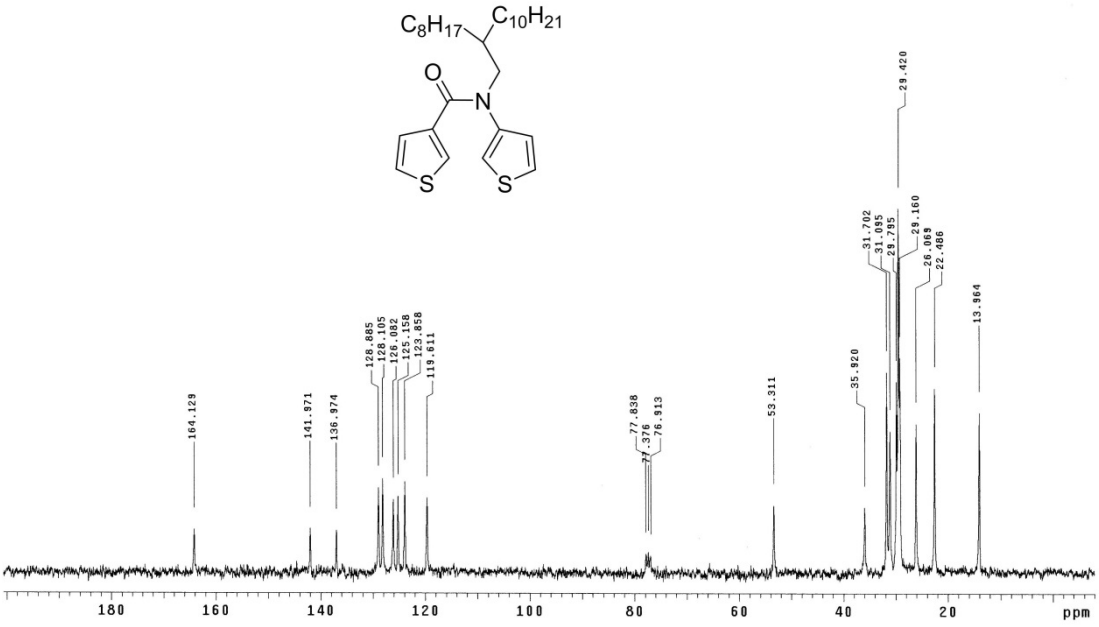

Fig. S10 [13]C NMR spectrum of **2** conducted in *d*-chloroform at 298K.

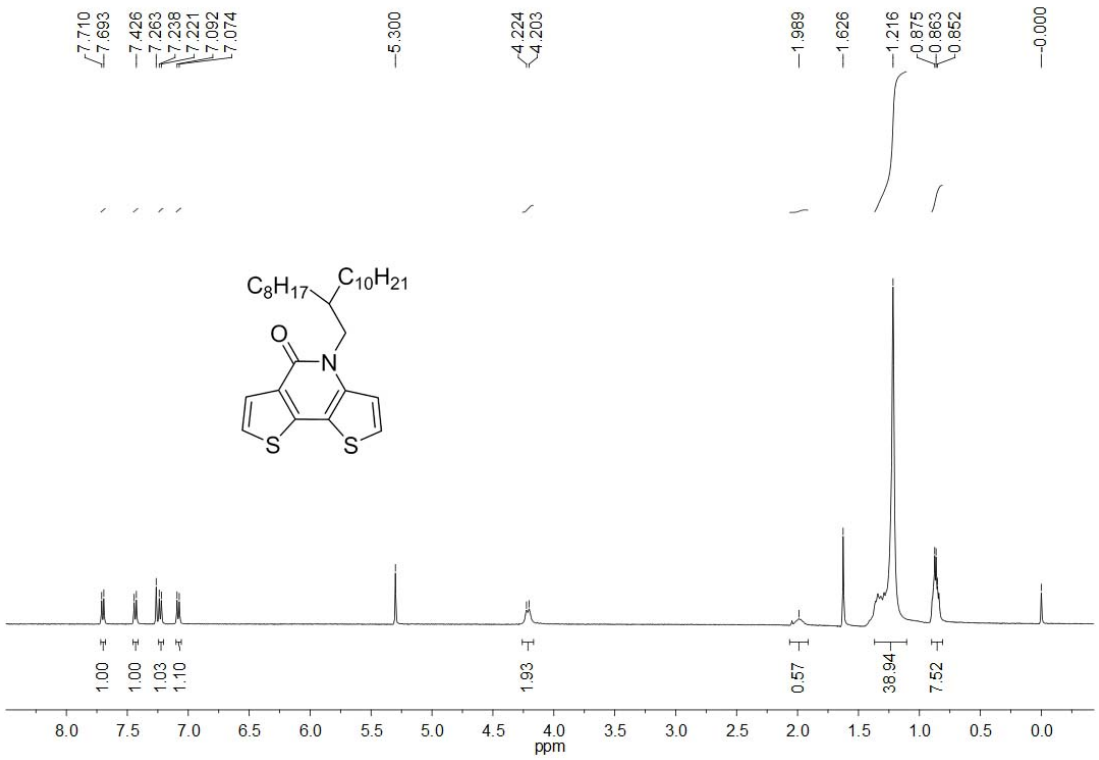

Fig. S11 [1]H NMR spectrum of DTPO conducted in *d*-chloroform at 298K.

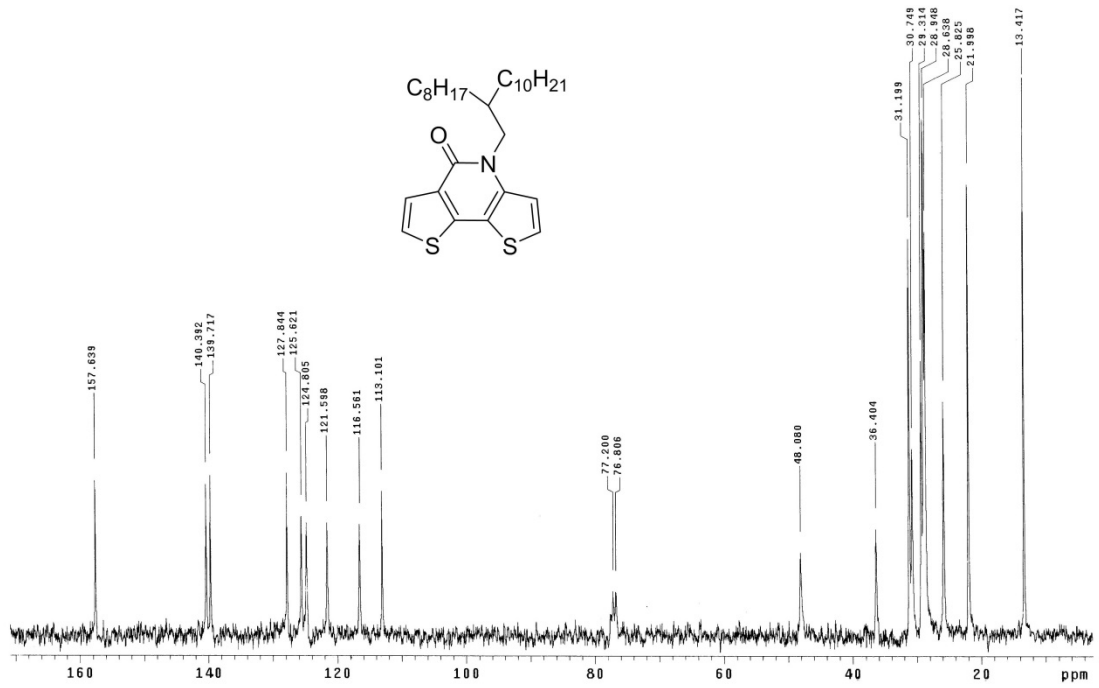

Fig. S12 [13]C NMR spectrum of DTPO conducted in *d*-chloroform at 298K.

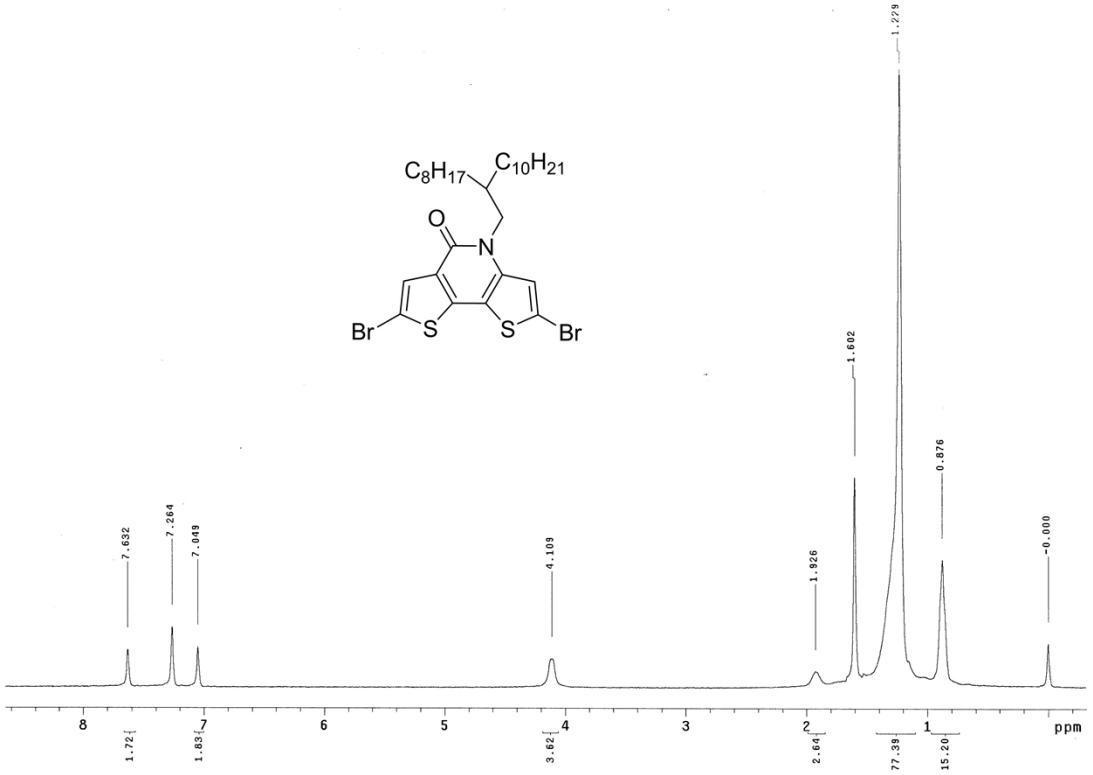

Fig. S13 ^{1}H NMR spectrum of M1 conducted in *d*-chloroform at 298K.

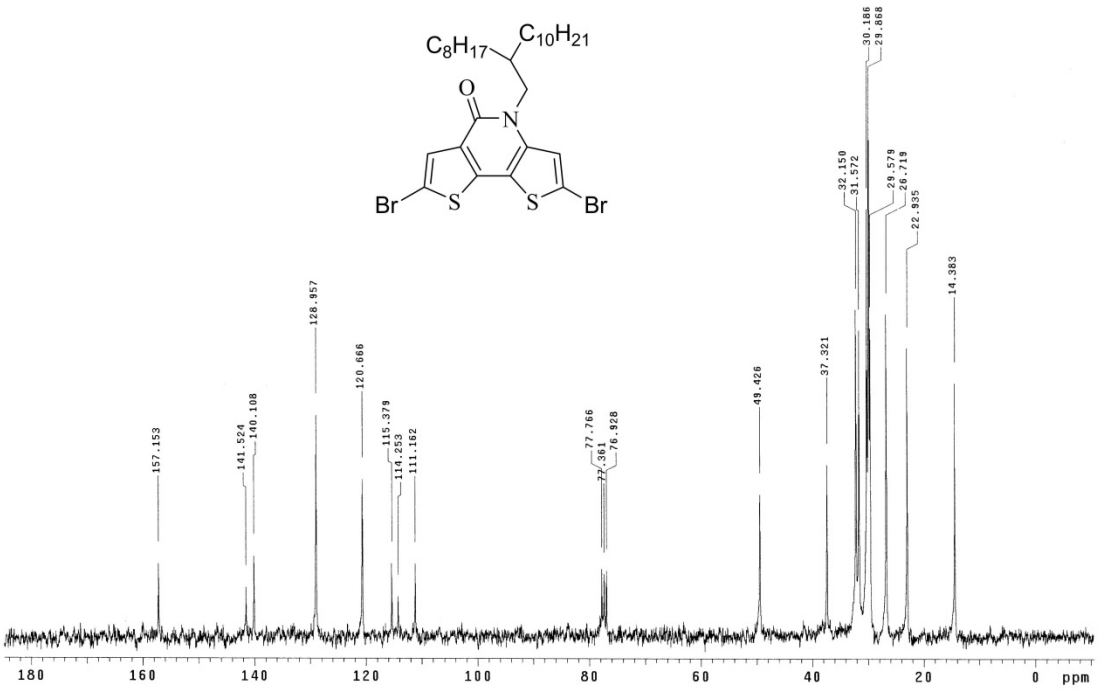

Fig. S14 ^{13}C NMR spectrum of M1 conducted in *d*-chloroform at 298K.

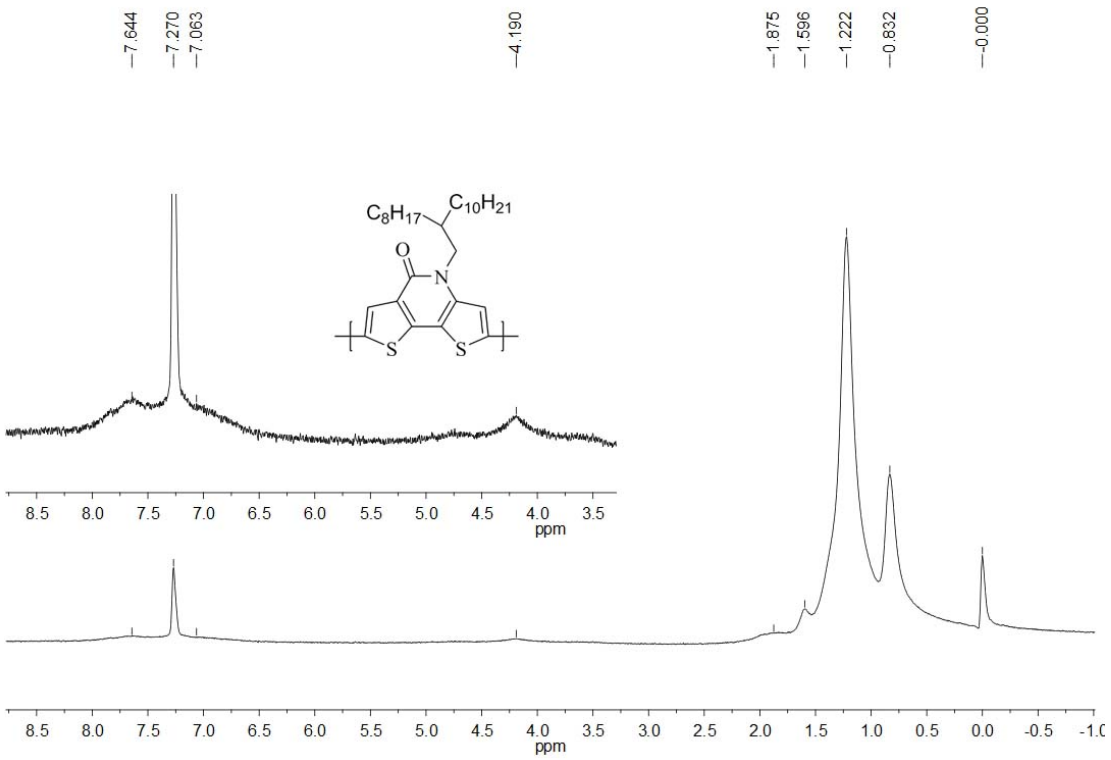

Fig. S15 [1]H NMR spectrum of PDTPO conducted in *d*-chloroform at 298K.

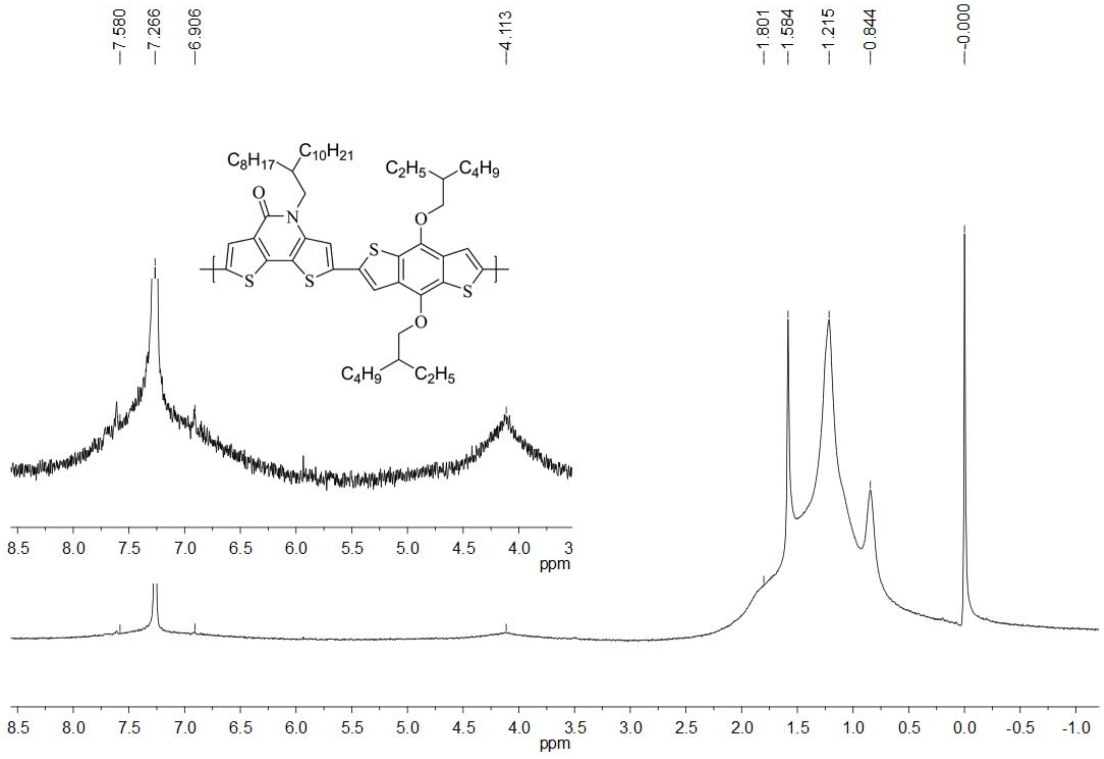

Fig. S16 [1]H NMR spectrum of PDTPO-BDTO conducted in *d*-chloroform at 298K.

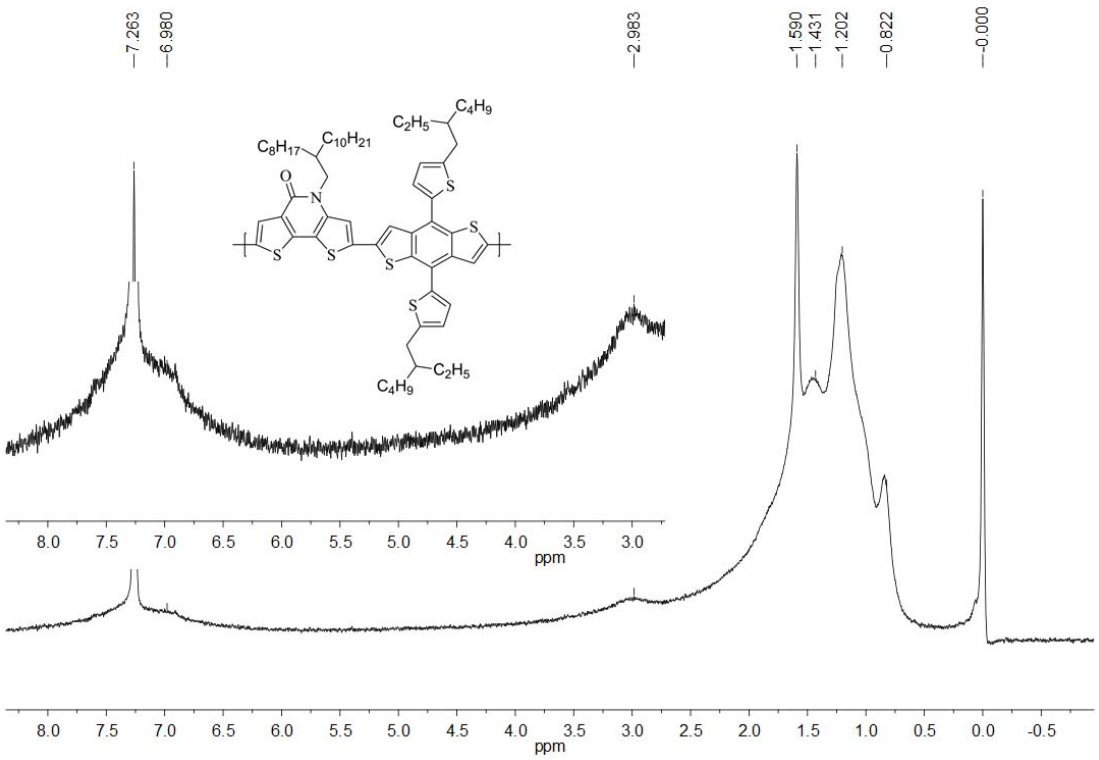

Fig. S17 ^{1}H NMR spectrum of PDTPO-BDTT conducted in *d*-chloroform at 298K.